

## Autonomous smart sensor nodes for global and local damage detection of prestressed concrete bridges based on accelerations and impedance measurements

Jae-Hyung Park<sup>1</sup>, Jeong-Tae Kim<sup>1\*</sup>, Dong-Soo Hong<sup>1</sup>, David Mascarenas<sup>2</sup>  
and Jerome Peter Lynch<sup>3</sup>

<sup>1</sup>Department of Ocean Engineering, Pukyong National University, Busan, Korea

<sup>2</sup>Los Alamos National Laboratory, Los Alamos, USA

<sup>3</sup>Department of Civil and Environmental Engineering, University of Michigan, USA

(Received October 14, 2009, Accepted April 1, 2010)

**Abstract.** This study presents the design of autonomous smart sensor nodes for damage monitoring of tendons and girders in prestressed concrete (PSC) bridges. To achieve the objective, the following approaches are implemented. Firstly, acceleration-based and impedance-based smart sensor nodes are designed for global and local structural health monitoring (SHM). Secondly, global and local SHM methods which are suitable for damage monitoring of tendons and girders in PSC bridges are selected to alarm damage occurrence, to locate damage and to estimate severity of damage. Thirdly, an autonomous SHM scheme is designed for PSC bridges by implementing the selected SHM methods. Operation logics of the SHM methods are programmed based on the concept of the decentralized sensor network. Finally, the performance of the proposed system is experimentally evaluated for a lab-scaled PSC girder model for which a set of damage scenarios are experimentally monitored by the developed smart sensor nodes.

**Keywords:** autonomous; wireless; smart sensor node; prestressed concrete bridge; structural health monitoring.

### 1. Introduction

Structural health monitoring (SHM) systems are widely adopted to monitor the structural responses, to detect damage, and to assess the effect of damage on the structural integrity. Many researchers have developed novel sensing technologies and damage monitoring techniques for the practical SHM applications. The SHM system for long-span bridges mainly includes a number of sensors, a huge amount of signal transmitting wires, data acquisition (DAQ) instruments, and one or more centralized data storage servers. The stored data in the centralized servers are handled for off-line signal and information analysis for damage monitoring and safety evaluation. However, the costs associated with installation and maintenance of SHM systems can be very high. The high costs associated with wired SHM systems can be greatly reduced through the adoption of wireless sensors (Straser and Kiremidjian 1998, Spencer *et al.* 2004, Lynch *et al.* 2006, Nagayama *et al.*

\*Corresponding Author, Professor E-mail: [idis@pknu.ac.kr](mailto:idis@pknu.ac.kr)

2007, Krishnamurthy *et al.* 2008, Cho *et al.* 2008). One of great advantages for using wireless sensors is that autonomous operations for the SHM can be implemented by embedding advanced system technologies. Therefore, the new paradigm by adopting smart sensor nodes may offer an autonomous and cost-efficient SHM.

For the autonomous and cost-efficient SHM, the development of wireless sensor nodes as much as the selection of embedding SHM algorithms are important topics (Lynch *et al.* 2003, Nagayama 2007, Wang *et al.* 2007, Zimmerman *et al.* 2008, Lu *et al.* 2008). To date, many SHM algorithms have been developed to monitor the location and the severity of damage in structures (Adams *et al.* 1978, Stubbs and Osegueda 1990, Yun and Bahng 2000, Kim *et al.* 2001, 2002, 2003a, 2003b, 2010). Most of the SHM algorithms are dependent on structural types, damage characteristics and available response signals. In this study, prestressed concrete (PSC) bridges were selected as the target structural type. For the PSC bridges, the prestress force in tendon and the structural properties (i.e., mass, damping and stiffness) in concrete girder are important parameters that should be secured for its serviceability and safety against external loadings and environmental conditions.

Since 1990s, several researchers have focused on using vibration characteristics of a PSC bridge as an indication of its structural damage (Saiidi *et al.* 1994, Miyamoto *et al.* 2000, Kim *et al.* 2004, Jeyasehar and Sumangala 2006). Based on the previous works, however, vibration-based approaches cannot easily distinguish the two damage-types, girder damage and tendon damage, unless the information on real damages is known. The pattern of one damage-type is hard to be distinguished from another since the change in vibration characteristics may be attributed to both damage-types. These make the vibration-based structural health monitoring difficult with a single sensing device to extract vibration characteristics. Therefore, other nondestructive evaluation techniques which are complementary to vibration-based approaches should be sought.

Recently, electro-mechanical impedance-based monitoring has shown the promising success to detect minor incipient change in structural integrity at local subsystems (Liang *et al.* 1994, Sun *et al.* 1995, Park *et al.* 2000, Bhalla and Soh 2003, Park *et al.* 2006). Compared to vibration-based approaches, the impedance-based method has the capability of more precisely locating damage such as crack and prestress-loss on small scale. Moreover, its local monitoring cannot characterize the entire structure, which means the global healthy state would not be easily captured to couple with the local monitoring information. Using those characteristics of the impedance-based methods, Kim *et al.* (2006) first proposed a combined SHM system with global vibration-based techniques and local impedance-based techniques. Also, Kim *et al.* (2009) used the combined system for prestress-loss monitoring in PSC bridges and Kim *et al.* (2010) proposed a serial hybrid SHM scheme using the global and local techniques for monitoring of PSC bridges.

This study presents the design of autonomous smart sensor nodes for damage monitoring of tendons and girders in PSC bridges. In order to achieve the objective, the following approaches are implemented. Firstly, acceleration-based and impedance-based smart sensor nodes are designed for global and local SHM. Secondly, global and local SHM methods which are suitable for damage monitoring of tendons and girders in PSC bridges are selected to alarm damage occurrence, to locate damage and to estimate severity of damage. Thirdly, an autonomous SHM scheme is designed for PSC bridges by implementing the selected SHM methods. Operation logics of the SHM methods are programmed based on the concept of the decentralized sensor network. Finally, the performance of the proposed system is experimentally evaluated for a lab-scaled PSC girder model.

## 2. Design of smart sensor nodes

A smart sensor node is defined as a sensor node with the following five essential features (Nagayama 2007): 1) on-board microprocessor, 2) sensing capability, 3) wireless communication, 4) battery powered and 5) low cost. Therefore, the smart sensor node should be composed of sensors, data acquisition unit, embedded software for damage detection and wireless radio. The data acquisition system includes amplifier, anti-aliasing filter and microcontroller. The on-board computation capacity of the microcontroller satisfies for signal processing as well as information analysis for damage monitoring.

### 2.1 Acceleration-based smart sensor node

Based on the original design of wireless sensor node by Lynch *et al.* (2006), in this study, an acceleration-based smart sensor node (Acc-SSN) was designed by modifying anti-aliasing filter, MEMS (micro electro-mechanical system) accelerometer and wireless radio capacity. As shown in Fig. 1, the Acc-SSN was consisted of eight (8) components: power supply, MEMS accelerometer, coupling capacitor, amplifier, anti-aliasing (AA) filter, analog-to-digital (A/D) converter, microcontroller and wireless radio. Coupling capacitor was designed by using a high pass-filter with a cutoff-frequency of 0.1 Hz. An operational amplifier (OP-AMP) was used to amplify low-level signals such as ambient vibration signals of civil structures.

For civil structures, high-resolution A/D converters are broadly employed for SHM systems. Even though the microcontroller has an embedded A/D converter of 10 bits and 8 channels, its resolution is relatively low due to quantization error. In order to solve the problem, a four-channel 16-bit A/D converter ADS8341 (Texas Instruments Inc.) was utilized. The performance of ADS8341 was evaluated by Lynch *et al.* (2006). An 8-bit microcontroller ATmega128 (ATMEL co.) with low-power consumption and low-cost was selected for the Acc-SSN. The microcontroller runs for multiple tasks which include operation schedule, system control (e.g., A/D converter and wireless radio), and radio transmission. The ATmega128 has the capacity enough to perform signal processing and information analysis based on 4-byte floating-point computation. Lynch *et al.* (2003) evaluated the computational capacity of ATmega128 for embedded fast Fourier transform (FFT) and autoregressive (AR) model. For signal processing and information analysis, an external memory of 32 kB was adopted for the sensor nodes.

For large civil infra-structures, long-range wireless radios are generally required to ensure that smart sensor nodes can be spaced adequate distances apart. Lynch *et al.* (2006) selected a wireless radio 9XCite (Digi International Inc.) of 900 MHz frequency for monitoring of large civil structures. In Korea, however, wireless radios using 2.4 GHz frequency band are legally allowed to be used outdoor. Therefore, we selected a wireless radio using 2.4 GHz frequency, XBee<sup>TM</sup> (Digi International Inc.). The outdoor line-of-sight range of the wireless radio is up to 100 m. The power requirements

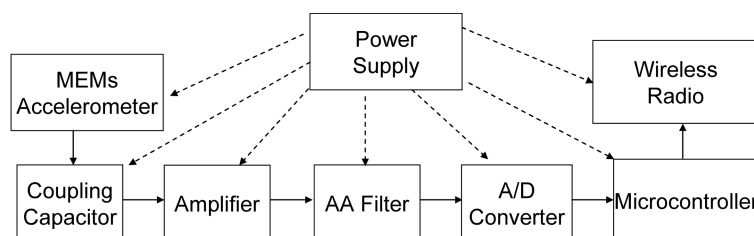


Fig. 1 Schematic of acceleration-based smart sensor node (Acc-SSN)

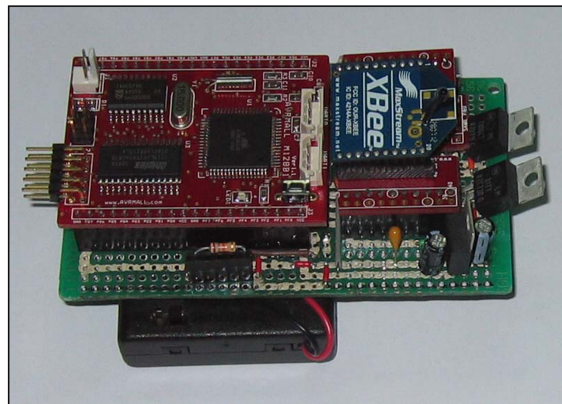


Fig. 2 Prototype of developed Acc-SSN

of the radio are 45 mA @ 3.3 V, 50 mA @ 3.3 V and 0.01 mA @ 3.3 V when transmitting, receiving and sleep-mode, respectively. As an anti-aliasing (AA) filter, the Butterworth low-pass filter was selected to avoid the aliasing problem. Butterworth low-pass filter is often used as anti-aliasing filter in data converter applications in which precise signal levels are required across the entire band-pass. An 8<sup>th</sup> order Butterworth low-pass filter with a cut-off frequency of 100 Hz was designed for SHM applications in civil structures.

For SHM in civil structures, ICP (integrated circuit piezoelectric) accelerometers have been broadly used due to their robustness with low-noise and high sensitivity characteristics. However, the ICP accelerometers are not suitable for smart sensor applications since they are expensive and also consume too much electrical-power relatively. Recently, MEMS accelerometers have been

Table 1 Comparison of acceleration-based smart sensor nodes

Sensor Node	Lynch <i>et al.</i> (2006)	Acc-SSN (this study)
Microcontroller	ATmega128L (Atmel) - Bus Size: 8 bits - Clock Speed: 0 - 8 MHz - Flash: 128 kB - RAM: 128 kB (Ext.) - Power: 2.7-5.5 V / 5.5 mA@Active 4 MHz	ATmega128 (Atmel) - Bus Size: 8 bits - Clock Speed: 0 - 16 MHz - Flash: 128 kB - RAM: 32 kB (Ext.) - Power: 4.5-5.5 V / 19 mA@Active 8 MHz
A/D Converter	ADS8341 (Texas Instruments) - Resolution: 16 bits	ADS8341 (Texas Instruments) - Resolution: 16 bits
AA Filter	4-pole Bassel Filter	8-pole Butterworth Filter
Accelerometer	3801D1FB3G (PCB Piezotronics) - Sensitivity: 700 mV/g - Range: $\pm 1.5$ g - Bandwidth: 80 Hz - Noise Floor: $150 \mu\text{V}/\sqrt{\text{Hz}}$	SD1221 (Silicon Designs) - Sensitivity: 2000 mV/g - Range: $\pm 2$ g - Bandwidth: 400 Hz - Noise Floor: $5 \mu\text{V}/\sqrt{\text{Hz}}$
Radio	9XCite (Digi International) - Radio Freq.: 900 MHz - Data Rate: up to 57.6 kbps - outdoor range: 300 m - Power: 2.85 - 5.5V / 35 mA(RX), 50 mA(TX)	XBee (Digi International) - Radio Freq.: 2.4 GHz - Data Rate: up to 250 kbps - outdoor range: 100 m - Power: 2.8 - 3.4 V / 50 mA(RX), 45 mA(TX)

developed for low costs, low power consumption and small size. Many researchers have attempted to implement the MEMS sensors for SHM in civil infra-structures. (Lynch *et al.* 2003, Ruiz-Sandoval *et al.* 2006, Nagayama 2007, Rice and Spencer 2008). In this study, SD1221 (by Silicon Design Inc.) was selected for its high-sensitivity (2000 mV/g), low-noise density ( $5 \mu\text{g}/\sqrt{\text{Hz}}$ ), and low-cost. Fig. 2 shows a prototype of the Acc-SSN developed in this study. The Acc-SSN consists of 2 layers as depicted in Fig. 2. The lower layer includes power supply (i.e., 6 V by 4 AAA batteries with 1.5 V for each battery), amplifier, AA filter, and A/D converter, while the upper layer functions for microcontroller and wireless radio chip. As summarized in Table 1, the specification of the developed Acc-SSN was compared with one by Lynch *et al.* (2006).

## 2.2 Impedance-based smart sensor node

Mascarenas *et al.* (2007) has worked on design of impedance-based smart sensor node (Imp-SSN). The design of the Imp-SSN is simpler than the Acc-SSN due to the multi-functional capability of AD5933 (Analog Devices) impedance chip. The AD5933 impedance chip has the following embedded multi-functional circuits: function generator, digital-to-analog (D/A) converter, current-to-voltage amplifier, anti-aliasing filter, A/D converter and discrete Fourier transform (DFT) analyzer. The AD5933 outputs real and imaginary values of impedance for a target frequency of interest and transmits the values into a microcontroller.

As a modified version, an Imp-SSN was designed as shown in Fig. 3. In the figure, two resistors are pull-up resistors for two wired interface (TWI) communication. The Imp-SSN was consisted of power supply, PZT sensor, impedance chip, microcontroller, and wireless radio. The same microcontroller (i.e., ATmega128) and wireless radio (i.e., XBee<sup>TM</sup>) used for the Acc-SSN were also adopted for the

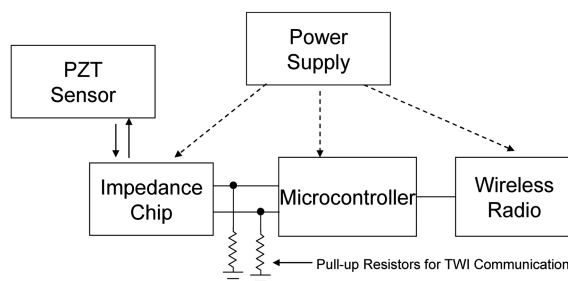


Fig. 3 Schematic of impedance-based smart sensor node (Imp-SSN)

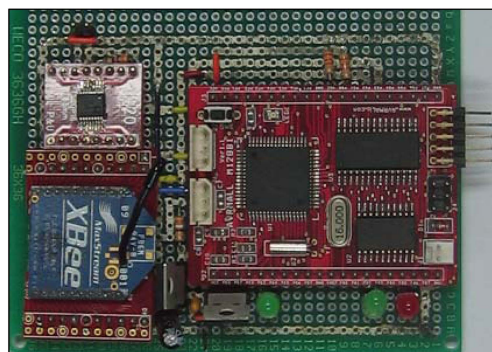


Fig. 4 Prototype of developed Imp-SSN

Table 2 Specification of impedance-based smart sensor node (Imp-SSN) and commercial impedance analyzer (HIOKI 3532-50)

Impedance analyzer	Imp-SSN	HIOKI 3532-50
Impedance range	1 kΩ - 10 MΩ	10 mΩ - 200 MΩ
Frequency range	1 kHz - 100 kHz	42 Hz - 5 MHz
Excitation voltage	1.98 Vp-p	14 Vp-p
Cost	US \$ 100	US \$ 15,000

Imp-SSN. The microcontroller runs for multiple tasks which include operation schedule, system control (e.g., AD5933 impedance chip and wireless radio), and radio transmission. A prototype of the Imp-SSN developed in this study is shown in Fig. 4. As summarized in Table 2, the specification of the developed Imp-SSN was compared with a commercial impedance analyzer HIOKI3532-50 (HIOKI E.E. Co.). Note that the measureable frequency range of the Imp-SSN is quite narrower than the commercial impedance analyzer.

Output values from the AD5933 impedance chip should be calibrated by using a feedback resistor (RFB), sensing on-board temperature, and measuring a resistor for the calibration (Analog Devices 2009). Furthermore, the output values were calibrated by comparing to impedance signals of the commercial impedance analyzer, HIOKI3532-50.

### 3. SHM methods for PSC bridges

The selection of SHM methods for the smart sensor nodes should be based on target structures, their inherent damage types, and the variety of extracted features. In this study, global and local SHM methods which are suitable for monitoring of PSC bridges were selected to alarm the occurrence of damage, to detect the location of damage, and to estimate the severity of damage. The selected global SHM methods are frequency response ratio assurance criterion, prestress-loss prediction model, and modal strain-energy (MSE)-based damage index. Also, the selected local SHM method is an impedance-based method using root-mean-square deviation. For each SHM method, the theory of approach is described in detail.

#### 3.1 Frequency response ratio assurance criterion (FRRAC)

Kim *et al.* (2009) proposed a global damage alarming indicator using the displacement ratio in frequency domain (i.e., frequency-response-ratio, FRR) between two outputs at difference locations. A frequency-response-ratio (FRR) function between the locations  $i$  and  $i+1$  is defined as

$$FRR_{i, i+1}(\omega) = \frac{S_{i+1, i}(\omega)}{S_{i, i+1}(\omega)} = \frac{H_i(\omega)}{H_{i+1}(\omega)} \quad (1)$$

where  $H_i(\omega_k)$  and  $H_{i+1}(\omega_k)$  are frequency response functions (FRFs) measured at locations  $i$  and  $i+1$ , respectively; and  $S_{i+1, i}(\omega_k)$  and  $S_{i, i+1}(\omega_k)$  are cross-spectral and auto-spectral density functions, respectively. By comparing a frequency-response-ratio measured at an undamaged baseline state to the corresponding one at a subsequent damaged state, a frequency-response-ratio assurance criterion (FRRAC) can be defined as follows

$$FRRAC(b, d) = \frac{\{FRR_b^T FRR_d\}^2}{\{FRR_b^T FRR_b\} \{FRR_d^T FRR_d\}} \quad (2)$$

where the subscripts  $b$  and  $d$  denote the undamaged baseline state and its corresponding damaged state, respectively. Eq. (2) represents the linear relationship between the pre-damaged frequency-response-ratio,  $FRR_b$ , and the post-damage frequency-response ratio,  $FRR_d$ . The FRRAC equals to the unity if no damage. Otherwise, the FRRAC is less than the unity.

In real applications, however, the FRRAC may be less than 1.0 although damage is not occurred. This is due to experimental and environmental errors. In order to discriminate damage occurrence from those errors, the control chart analysis is utilized (Sohn *et al.* 2003). By noticing the nature of the FRRAC, the lower control limit (LCL) was adopted as follows

$$LCL_{FRRAC} = \mu_{FRRAC} - 3\sigma_{FRRAC} \quad (3)$$

where  $\mu_{FRRAC}$  and  $\sigma_{FRRAC}$  are mean and standard deviation of FRRACs, respectively. The occurrence of damage is indicated when the FRRAC is beyond (i.e., less than) the bound of the LCL. Otherwise, there is no indication of damage occurrence.

### 3.2 Prestress-loss prediction model

For PSC bridges, Kim *et al.* (2004) proposed a frequency-based prestress-loss prediction model based on the concept of equivalent flexural rigidity for cable under uniform tension. The relative change in prestress forces is estimated by the fractional change in natural frequencies measured from the PSC beam.

$$\left( \frac{\delta N}{N} \right)_n = \frac{\delta \omega_n^2 - \delta \varpi_n^2}{\omega_n^2 - \varpi_n^2} \quad (4)$$

where  $N$  is the prestress force;  $\omega_n$  is the eigenvalue for the  $n^{\text{th}}$  mode; and  $\varpi_n$  is the  $n^{\text{th}}$  eigenvalue of the beam with zero prestress force. From the Eq. (4), the relative change in prestress force can be estimated by measuring changes in natural frequency due to changes in prestress forces. Eq. (4) can be simplified by further assuming no change in concrete flexural rigidity occurred due to the prestress-loss, i.e.,  $\delta \varpi_n \approx 0$ . In existing real structures, however,  $\varpi_n$  may not be available unless measured at as-built state. As an alternative way,  $\varpi_n$  can be estimated from a numerical analysis using system identification process.

### 3.3 Modal strain energy-based damage index

Modal strain energy (MSE) is one of the damage sensitive features because it uses mode-shape curvatures. The MSE-based damage index method is based on the decrease in modal strain energy between two structural DOFs (Kim *et al.* 2003). The MSE-based damage index is defined as

$$\beta_j = \frac{E_j}{E_j^*} = \frac{[\Phi_i^{*T} \mathbf{K}_{j0} \Phi_i^*] K_i}{[\Phi_i^T \mathbf{K}_{j0} \Phi_i] K_i^*} \quad (5)$$

where  $\beta_j$  and  $E_j$  represent the MSE-based damage index and material stiffness for the  $j^{\text{th}}$  member, respectively. The symbol  $\Phi_i$  represent the  $i^{\text{th}}$  modal vector;  $\mathbf{K}_{j0}$  involves only geometric quantities; and

$K_i$  is  $i^{\text{th}}$  modal stiffness and the symbol (  $^*$  ) denotes damaged state. The damage indices are also normalized according to the standard rule as

$$Z_j = (\beta_j - \mu_\beta) / \sigma_\beta \quad (6)$$

where  $Z_j$  is the standard normalized damage index of the element  $j$ . The symbols  $\mu_\beta$  and  $\sigma_\beta$  represent the mean and standard deviation of the collection of  $\beta_j$  values, respectively. The beam elements are next assigned to a damage class by utilizing hypothesis testing. The null hypothesis (i.e.,  $H_0$ ) is taken to be the structure undamaged at the  $j^{\text{th}}$  element and the alternate hypothesis (i.e.,  $H_1$ ) is taken to be the structure damaged at the  $j^{\text{th}}$  element. In assigning damage to a particular location, the following decision rule was utilized: (1) choose  $H_1$  if  $Z_j \geq z_o$ ; and (2) choose  $H_0$  if  $Z_j < z_o$ , where  $z_o$  is number which depends upon the confidence level of the localization test. Then damage is assigned to a particular location  $j$  if  $Z_j$  exceeds the confidence level.

### 3.4 Root-mean-square-deviation (RMSD) of impedance signature

Impedance-based damage detection techniques utilize piezoelectric materials as sensors and actuators (Liang *et al.* 1994, Park *et al.* 2000, Bhalla and Soh 2003, Park *et al.* 2006). The electrical impedance of the piezoelectric patch bonded onto a host structure is directly related to the mechanical impedance of the structure. When damage occurs to a structure, its mechanical impedance will be changed. Hence, any changes in the electrical impedance signature (such as magnitude of admittance and resonant frequency) are attributed to damage or changes in the structure.

To quantify the change in impedance signature due to damage in the structure, the root-mean-square-deviation (RMSD) of impedance signatures measured before and after damage (Sun *et al.* 1995) was used in this study. The RMSD is calculated from impedance measurements before and after damage as

$$RMSD = \sqrt{\sum_{i=1}^N [Z^*(\omega_i) - Z(\omega_i)]^2 / \sum_{i=1}^N [Z(\omega_i)]^2} \quad (7)$$

where  $Z(\omega_i)$  and  $Z^*(\omega_i)$  are impedances measured before and after damage for  $i^{\text{th}}$  frequency, respectively; and  $N$  denotes the number of frequency points in the sweep. The RMSD equals to 0 if no damage. Otherwise, the RMSD is larger than 0.

Due to experimental and environmental errors, however, the RMSD may be larger than 0 although damage is not occurred. By noticing the nature of the RMSD values, the upper control limit (UCL) is adopted for alarming damage occurrence, as follows

$$UCL_{RMSD} = \mu_{RMSD} + 3 \sigma_{RMSD} \quad (8)$$

where  $\mu_{RMSD}$  and  $\sigma_{RMSD}$  are mean and standard deviation of RMSDs, respectively. The occurrence of damage is indicated when the RMSD values are beyond (i.e., larger than) the bound of the UCL. Otherwise, there is no indication of damage occurrence.

#### 4. Autonomous SHM scheme for smart sensor nodes

The autonomous SHM scheme used for smart sensor nodes are based on the decentralized wireless sensor network, as schematized in Fig. 5(b). Compared to the centralized sensor network as shown in Fig. 5(a), each sensor node in the decentralized network performs multiple tasks including acquiring signals, analyzing information and computing data for decision-making process. In this study, the autonomous SHM scheme includes three vibration-based SHM methods and one impedance-based SHM method, as described previously. Note that the vibration-based SHM methods are embedded in the acceleration-based sensor nodes (i.e., Acc-SSNs) and the impedance-based SHM method is embedded in the impedance-based sensor node (i.e., Imp-SSNs). For the autonomous SHM, operation logics of the SHM methods are programmed for embedding into the smart sensor nodes. Finally, an autonomous SHM scheme is designed for PSC bridges by implementing the operation logics of the SHM methods.

##### 4.1 Operation logics of SHM methods

###### 4.1.1 FRRAC

The operation logic of FRRAC was designed as shown in Fig. 6. For the FRRAC, two sensor nodes (i.e., Acc-SSN  $i$  and Acc-SSN  $j$ ) installed at damage-sensitive locations should be selected. The smart sensor nodes operate: 1) to acquire acceleration signals  $\{y_i(t) y_j(t)\}$ , 2) to compute frequency responses  $\{Y_i(\omega) Y_j(\omega)\}$ , 3) to calculate FRR of Eq. (1), 4) to calculate FRRAC of Eq. (2) and 5) to determine the occurrence of damage by control chart analysis (i.e., Eq. (3)).

###### 4.1.2 Prestress-loss prediction model

As shown in Fig. 7, the operation logic of prestress-loss prediction model was designed by using the peer-to-peer network. For the prestress-loss prediction model, one (1) sensor node (i.e., Acc-SSN  $i$ ) installed at a damage-sensitive location should be selected. Then, the smart sensor node operates: 1) to acquire acceleration signals  $y_i(t)$ , 2) to compute frequency response  $Y_i(\omega)$ , 3) to extract natural frequencies and 4) to estimate prestress-loss by the prestress-loss prediction model of Eq. (4).

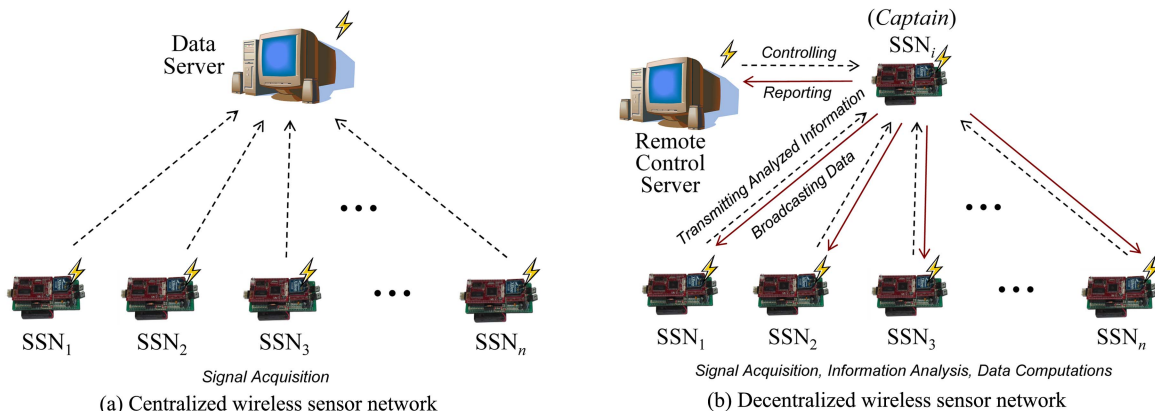


Fig. 5 Comparison of centralized and decentralized wireless sensor networks

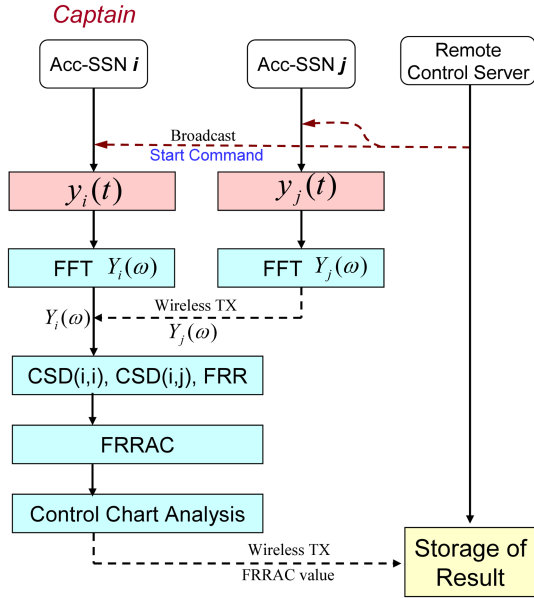


Fig. 6 Operation logic of FRRAC

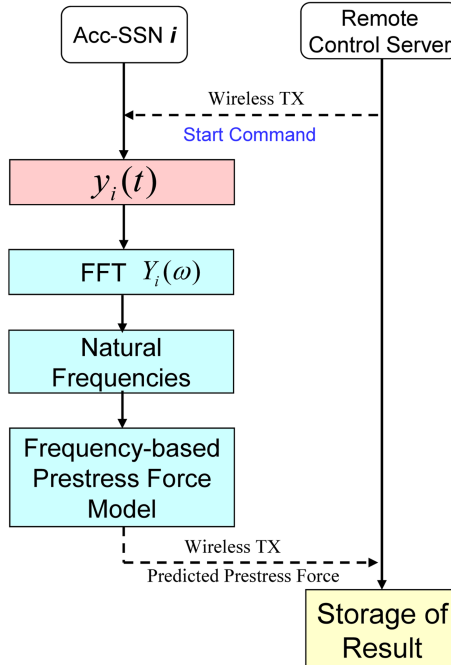


Fig. 7 Operation logic of prestress-loss prediction model

#### 4.1.3 MSE-based damage index

In order to calculate MSE-based damage index, modal parameters such as natural frequencies and mode shapes of a structure should be extracted. In this study, the frequency domain decomposition

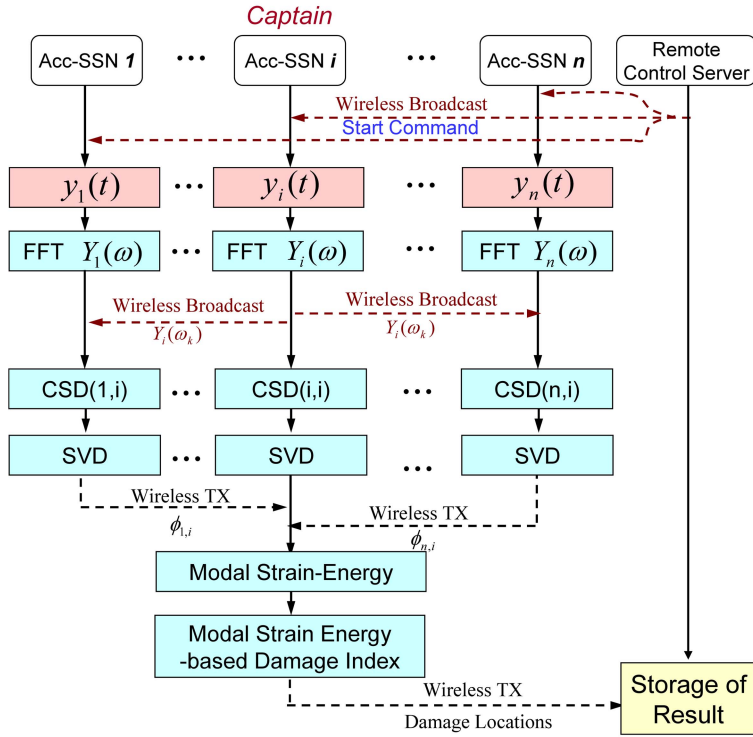


Fig. 8 Operation logic of MSE-based damage index

(FDD) technique (Yi and Yun 2004) was employed for modal parameter extraction. Based on the decentralized wireless sensor networks, the operation logic of MSE-based damage index was designed as shown in Fig. 8. The captain sensor node (Acc-SSN  $i$ ) should be located at a sensitive point in order to measure appropriate vibration modes with less noise effect. The smart sensor nodes operate: 1) to acquire acceleration signals  $\{y_k(t), k = 1, \dots, n\}$ , 2) to compute frequency responses  $\{Y_k(\omega), k = 1, \dots, n\}$ , 3) to compute cross-spectral densities between two FFT results  $\{CSD(k,i), k = 1, \dots, n\}$ , 4) to extract modal vectors by the FDD technique, 5) to assemble the received modal vectors and calculate MSEs and 6) to locate damage by using the MSE-based damage index (i.e., Eqs. (5) and (6)).

#### 4.1.4 RMSD of impedance signature

Based on the wireless sensor network, the operation logic of impedance-based method using RMSD was designed as shown in Fig. 9. The Imp-SSNs are installed near the tendons to monitor prestress-loss of PSC bridges. The smart sensor nodes operate: 1) to acquire impedance signatures  $\{Z_i(\omega), i = 1, \dots, n\}$ , 2) to compute RMSD of impedance features, 3) to determine the occurrence of damage by control chart analysis (i.e., Eq. (8)) and 4) to assemble the damage detection results and determine damaged members.

#### 4.2 Autonomous SHM scheme

Based on the hybrid SHM method proposed by Kim *et al.* (2010), a modified SHM scheme was

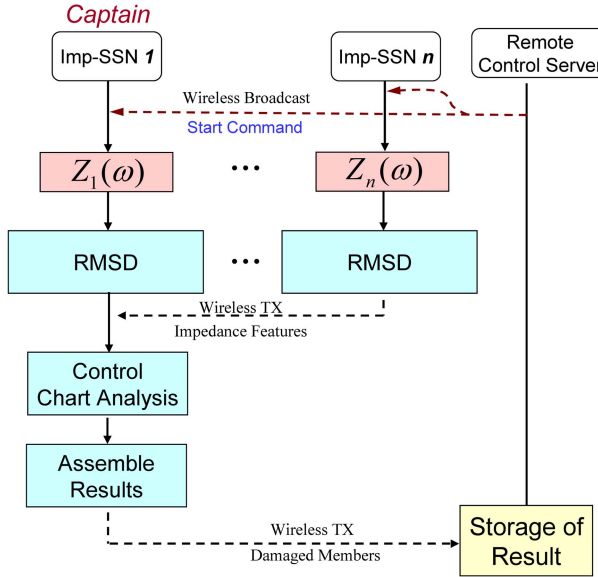


Fig. 9 Operation logic of impedance-based method using RMSD

designed to monitor PSC bridges. The basic idea of the scheme is that the global SHM method is used for alarming damage occurrence in global structure level and, at the same moment, the local SHM method is used for pin-pointing damage occurrence at prescribed local member level. Note that global methods using accelerations can detect structural changes (e.g., crack, added-mass and tension loss of tendon) from a sensor in an overall structure, while local methods using impedances can detect damage in only a specific structural member (or sub-structure) near an attached sensor. Then, the type of alarmed damage is classified by recognizing the patterns of the SHM results. In this study, the autonomous operation scheme for hybrid SHM was designed based on the four operation logics of SHM methods, as described previously (i.e., Figs. 6-9). The scheme consists of three phases, in which each operation phase is described in detail as follows:

#### Phase I: Global and local alarming process

- Step 1) Acc-SSNs and Imp-SSNs measure acceleration and impedance signals, respectively.
- Step 2) Acc-SSNs calculate frequency response ratio (FRR) of Eq. (1), natural frequencies, and mode shapes, and Imp-SSNs calculate RMSD of Eq. (7).
- Step 3) Acc-SSNs compute FRRAC indices of Eq. (2) and their control limits of Eq. (3) to monitor global damage alarming. Imp-SSNs calculate their control limits of Eq. (8) to monitor local damage alarming.

#### Phase II: Damage classification process

- Step 4) The captain Imp-SSN transmits local damage information to the captain Acc-SSN. Then, the captain Acc-SSN assembles the global and local damage information;
- Step 5) By making decision based on the global alarming of Acc-SSNs and the local alarming of Imp-SSNs, the captain Acc-SSN classifies the damage into one of four classes;
  - ① Class 1: '*No Damage Occurrence*' if the global alarming indicates '*OFF*' and the local alarming also indicates '*OFF*'.

- ② Class 2: ‘Occurrence of Girder Damage and Tendon Damage’ if the global alarming indicates ‘ON’ and the local alarming also indicates ‘ON’.
- ③ Class 3: ‘Occurrence of Girder Damage’ if the global alarming indicates ‘ON’ but the local alarming indicates ‘OFF’.
- ④ Class 4: ‘Occurrence of Minor Tendon Damage’ if the global alarming indicates ‘OFF’ but the local alarming indicates ‘ON’.

### Phase III: Detailed damage estimation process

Step 6) The captain Acc-SSN performs detailed damage estimation for the classified damage. Tendon damage is estimated by the frequency-based prestress-loss prediction model of Eq. (4). Girder damage is estimated by the MSE-based damage index of Eqs. (5) and (6).

Step 7) The captain Acc-SSN transmits the monitoring results to the Remote Control Server.

## 5. Experimental evaluation

### 5.1 Experimental setup and preliminary tests

A lab-scaled PSC girder model was used to verify the proposed autonomous operation schemes using the smart sensor nodes. The girder with T-beam section has the span length of 6 m (see the Kim *et al.* (2010) for detailed description on the structure). Locations and arrangements of the acceleration-based smart sensor nodes (Acc-SSNs) and conventional accelerometers on the test structure were designed as shown in Fig. 10. Seven Acc-SSNs (Acc-SSN 1–7) were placed along the girder with constant interval. As shown in Fig. 10, seven conventional accelerometers PCB393B04 (PCB 1–7) were also located at the side of the Acc-SSNs. The conventional accelerometers were used to compare the performance of the developed Acc-SSNs.

The impact excitation was applied by an electro-magnetic shaker (VTS100) at a location 1.7 m distanced from the right edge. Impact force, which has 444.5 N intensity, was applied to the PSC girder by the electro-magnetic shaker. As shown in Fig. 11(a), dynamic responses in vertical direction were measured from the Acc-SSNs and the corresponding 7 commercial sensors with a sampling frequency of 500 Hz. The commercial data acquisition system includes a 16-channel signal conditioner (PCB 481A03), a 16 channel DAQ (NI-6036E) card, and a laptop with MATLAB. Fig. 11(b) shows frequency responses acquired from the Acc-SSNs and the commercial system. The

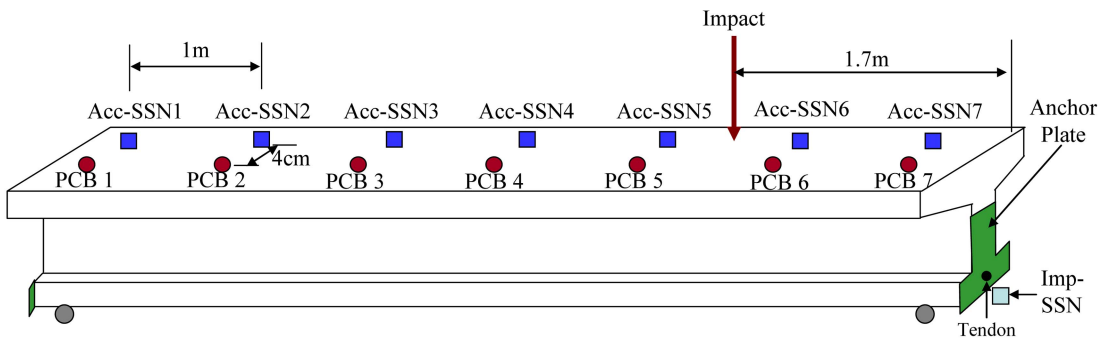


Fig. 10 Arrangement of Acc-SSNs and conventional PCB accelerometers

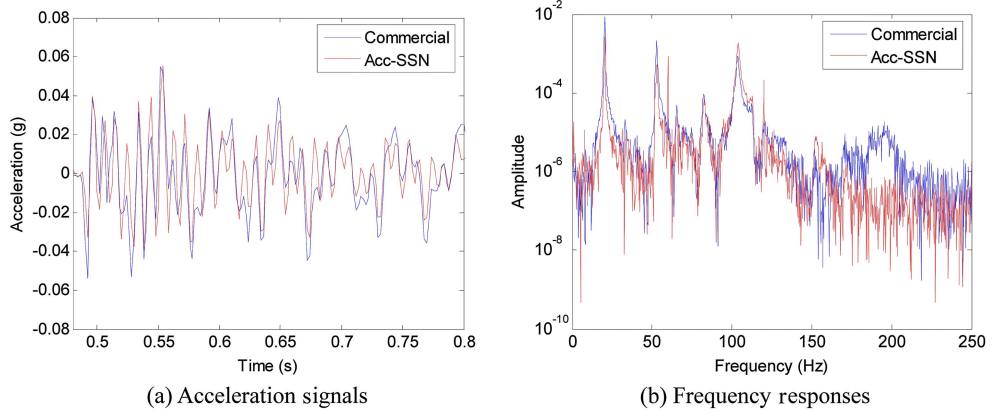


Fig. 11 Experimental results of Acc-SSN 5 and commercial accelerometer (PCB 5)

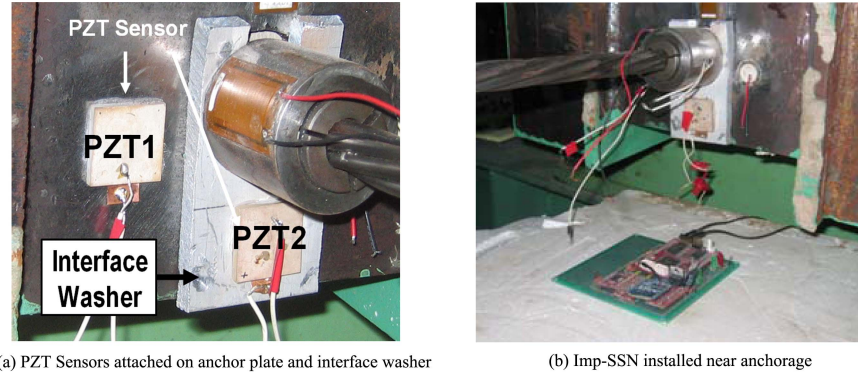


Fig. 12 PZT sensors and Imp-SSN installed on PSC girder model

responses from the Acc-SSNs and the commercial system show good matches with little difference.

For impedance measurement, two PZT sensors, PZT 1 and PZT 2, were placed on the anchor plate and the interface washer, respectively, as shown in Fig. 12(a). In this study, an aluminum plate was installed as the interface washer between the anchor plate and the wedge of tendon. The interface washer was specially adopted to improve the sensitivity of the Imp-SSN which has the limited measurable frequency range. The PZT sensors, both PZT 1 and PZT 2, were  $25 \times 25$  mm, PZT 5A type patch. Also, the Imp-SSN was placed near the PZT sensors as shown in Fig. 12(b). A set of sweep tests was performed by using a commercial impedance analyzer in order to determine the range for frequency sweep between 10 kHz and 100 kHz. The commercial data acquisition system includes an impedance analyzer HIOKI 3532, a GPIB interface, and a laptop computer with LabVIEW software. The input voltage into the PZT sensor by the HIOKI 3532 was set up as  $1.98 V_{p-p}$ , which is the same as the maximum output voltage of the Imp-SSN as listed in Table 2.

Fig. 13(a) shows the impedance signatures measured from the PZT 1 sensor on the anchor plate. In the figure, no peak point was meaningfully recurred, from repeated measurements, in the scanned 10 kHz - 23 kHz frequency range. Fig. 13(b) shows the impedance signatures measured from the PZT 2 sensor on the interface washer. In the figure, a recurring peak point, from repeated sweep tests, was found in a narrow range of 16.5 - 17.5 kHz in the scanned 10 kHz - 23 kHz frequency range.

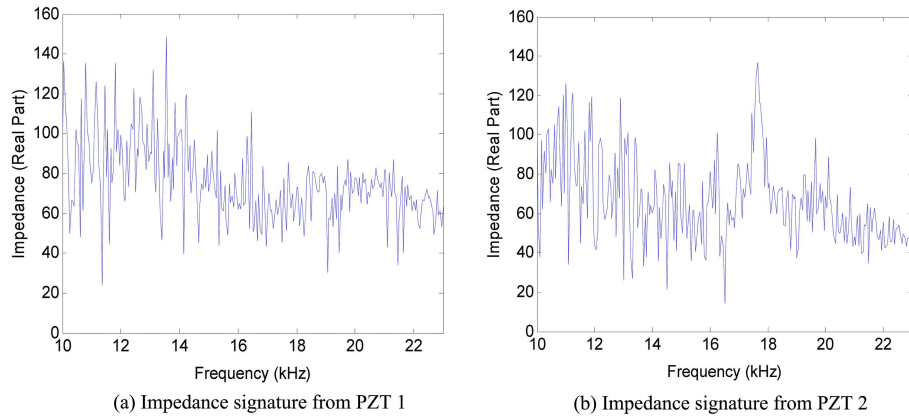


Fig. 13 Impedance signatures measured between 10 kHz - 23 kHz

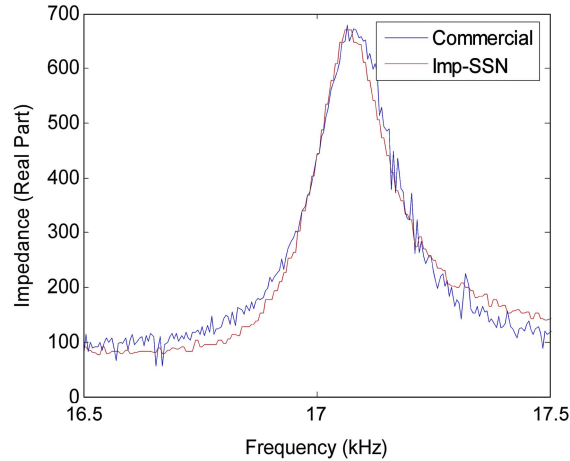


Fig. 14 Impedance signatures measured from PZT 2 by commercial impedance analyzer and Imp-SSN

From these sweep test results, the PZT 2 sensor on the interface washer was selected to monitor the change in impedance signatures due to damage occurrence in tendon-anchor subsystems. From the measurements by the Imp-SSN and the commercial analyzer, as shown in Fig. 14, a feasible peak point was coincided at 17.1 kHz in the narrow frequency range of 16.5 - 17.5 kHz. Those two impedance signals show good matches with little difference. The change in impedance signatures due to change in structural condition is more sensitive near the peak point.

Table 3 Damage scenarios for girder and tendon (GT)

Damage case	Prestress force (kN)	Girder damage	
		Added Mass (kN)	Location (m)
Undamaged	98.0	-	-
GT1	98.0	1.2	2.7 - 3.2
GT2	88.2	0	-
GT3	78.4	2.4	2.7 - 3.2

As shown in Table 3, a few mixed damage scenarios combining girder damage and tendon damage. Damage scenarios are three cases: GT1, GT2 and GT3. The first damage case (GT1) is to simulate the girder damage by added mass (Kim *et al.* 2010). The added mass may not be referred as damage; however, it was treated as a damaging event for the evaluation purpose since the increment of mass results in similar effect as the decrement of stiffness caused by a crack. The second damage case (GT2) is to introduce tendon damage by prestress-loss. The last case (GT3) is to simulate girder and tendon damages simultaneously occurred in the PSC girder model.

### 5.2 SHM results of smart sensor nodes

For the three damage cases (i.e., GT1, GT2 and GT3), the autonomous operation scheme embedded in the smart sensor nodes were performed for damage occurrence monitoring, damage classification, and detailed damage estimation for the PSC girder model. The seven Acc-SSNs shown in Fig. 10 were used for the global health monitoring. Also, an Imp-SSN installed only at the tendon anchor as shown in Figs. 10 and 12 was used for the local health monitoring.

For the damage case GT1, as shown in Fig. 15, the global alarming results and the local monitoring results were obtained by the Acc-SSNs and the Imp-SSN, respectively. First, FRRAC values were obtained from Acc-SSN5 and Acc-SSN6. As shown in Fig. 15(a), the monitored FRRAC values are beyond the bound of lower control limit (LCL). This indicates that the damage is globally alarmed by the Acc-SSNs. Next, as shown in Fig. 15(b), the RMSD values monitored from the Imp-SSN are within the bound of upper control limit (UCL). This indicates that the damage is not locally alarmed by the Imp-SSNs. Upon receiving monitoring results (i.e., Global Alarming ‘ON’ and Local Alarming ‘OFF’ as described in Chapter 4), the captain Acc-SSN5 classified the situation as ‘*Class 3: Occurrence of Girder Damage*’, as categorized in Section 4.2. Next, Acc-SSNs performed the detailed damage estimation by using the MSE-based damage index method for girder damage. As shown in Fig. 15(c), the damage was accurately located by the MSE-based damage index method embedded in the captain Acc-SSN5.

For the damage case GT2, as shown in Fig. 16, the damage alarming results were obtained by the Acc-SSNs and the Imp-SSN, respectively. First, as shown in Fig. 16(a), the FRRAC values are beyond the LCL bound. Next, as shown in Fig. 16(b), the RMSD values are also beyond the UCL bound. Note that the LCL and UCL values in Figs. 16(a) and (b) were recalculated from measured data after removing the added mass in the damage case GT1, so that the values are different from the values in Figs. 15(a) and (b). Upon receiving those monitoring results (i.e., Global Alarming ‘ON’

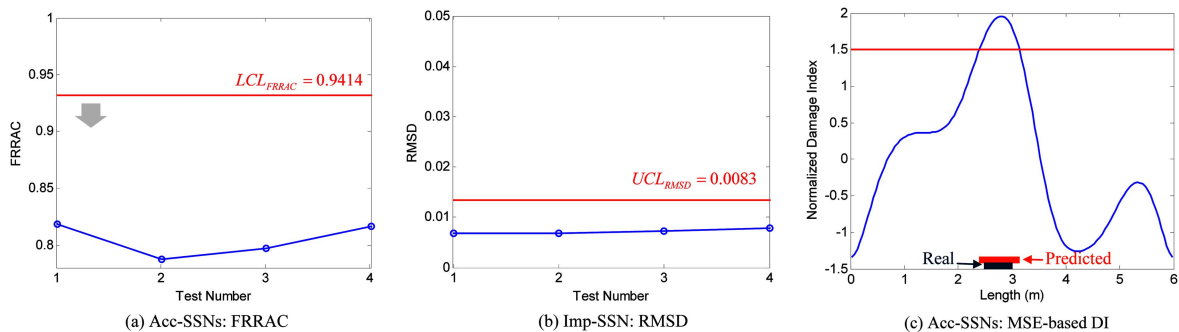


Fig. 15 SHM results for damage case GT1

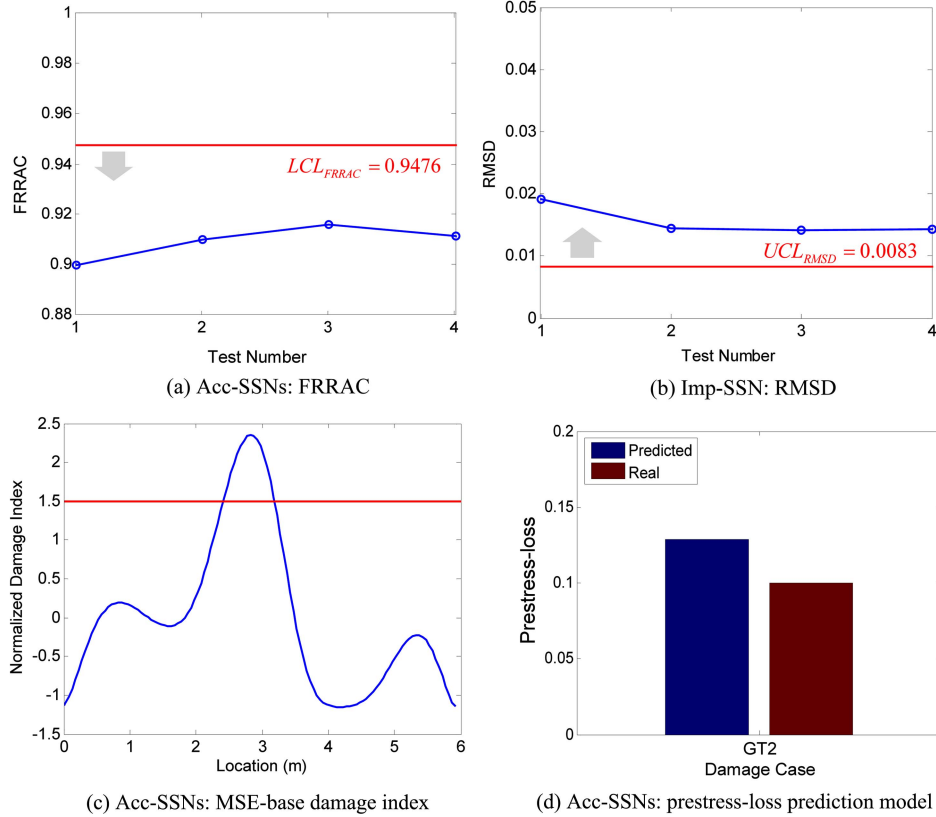


Fig. 16 SHM results for damage case GT2

and Local Alarming ‘ON’), the captain Acc-SSN5 classified the situation as ‘*Class 2: Occurrence of Tendon Damage and Girder Damage*’. Next, Acc-SSNs performed the detailed damage estimation by using both the MSE-based damage index method for girder damage and the frequency-based prestress-loss prediction model for tendon damage. Fig. 16(c) shows damage estimation results by the MSE-based damage index method. Fig. 16(d) shows damage estimation results by the prestress-loss prediction model. The tendon damage was estimated with good accuracy; however, the girder damage was indicated near mid-span even though there was no girder damage inflicted to the test (i.e., false positive prediction).

For the damage case GT3, as shown in Fig. 17, the damage alarming results were obtained by the Acc-SSNs and the Imp-SSN, respectively. The FRRAC values were beyond the LCL bound as indicating the occurrence of global damage. The RMSD values were beyond the UCL bound, as also indicating the local damage occurrence. Note that the LCL and UCL values in Figs. 17(a) and (b) were recalculated from measured data after resetting the reduced prestress-force in the damage case GT2, so that the values are different from the values in Figs. 16(a) and (b). Upon receiving those monitoring results (i.e., Global Alarming ‘ON’ and Local Alarming ‘ON’), the captain Acc-SSN5 classified the event as ‘*Class 2: Occurrence of Tendon Damage and Girder Damage*’. Next, the Acc-SSNs performed detailed damage estimation as shown in Figs. 17(c) and (d), respectively. Fig. 17(c) shows damage estimation results by the MSE-based damage index method. Fig. 17(d) shows

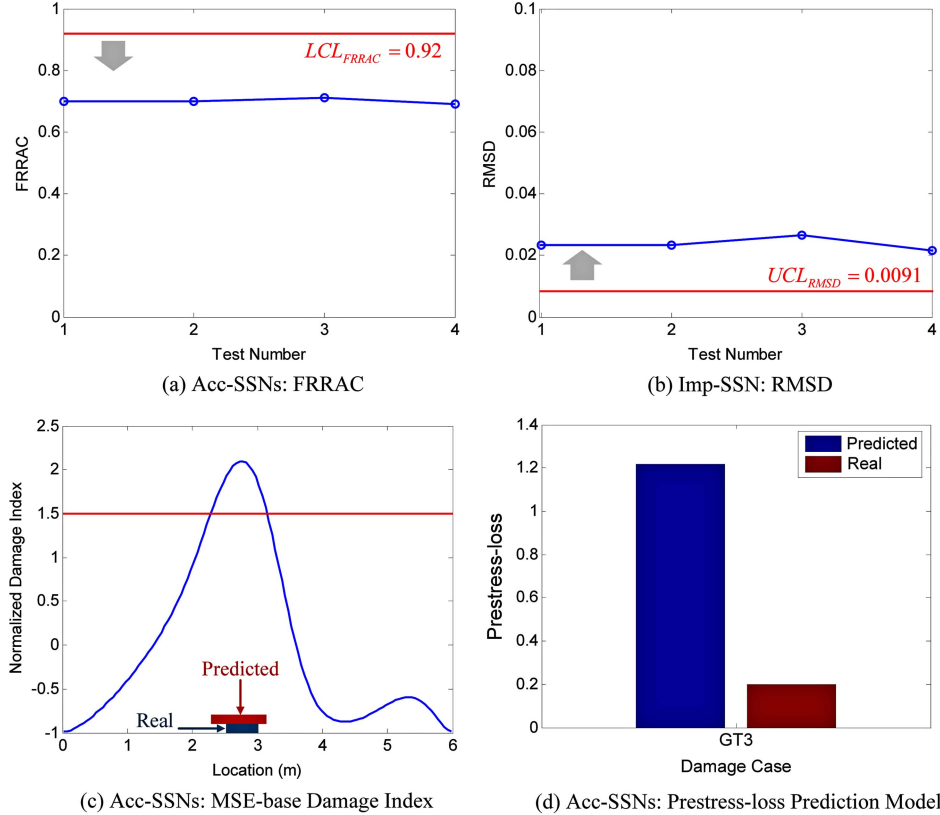


Fig. 17 SHM results for damage case GT3

damage estimation results by the prestress-loss prediction model. The girder damage was located with good accuracy; however, the tendon damage was estimated with very large error since the girder damage as well as the tendon damage causes the change in natural frequencies of the PSC girder model.

## 6. Conclusions

In this study, autonomous smart sensor nodes were designed for damage monitoring of tendons and girders in PSC bridges. To achieve the objective, the following approaches were implemented. Firstly, acceleration-based and impedance-based smart sensor nodes were designed for global and local SHM. Secondly, global and local SHM methods suitable for damage monitoring of tendons and girders in PSC bridges were selected. Thirdly, an autonomous SHM scheme was designed for PSC bridges by implementing the selected SHM methods. Operation logics of the SHM methods were programmed based on the concept of the decentralized sensor network. Finally, the performance of the proposed system was experimentally evaluated in a lab-scaled PSC girder model.

From the experimental evaluation, the smart sensor nodes accurately alarmed the occurrence of damage in tendon and girder of the PSC girder model. In the case of girder damage, the smart sensor nodes successfully classified its damage type and detected damage location with good accuracy. In

the case of tendon damage, the prestress-loss was estimated with good accuracy; however, the girder damage was false-alarmed. In the mixed case of tendon damage and girder damage, the girder damage was located near mid-span with good accuracy but the prestress-loss was estimated with relatively large error.

In order to improve the accuracy of damage estimation, the autonomous SHM scheme embedded in smart sensor nodes should be improved to appropriately reflect the mixed damage scenarios of the PSC bridges. Furthermore, the smart sensor nodes should be improved for field applications by dealing with temperature-induced uncertainty and power management problem. Energy harvesting may be considered in conjunction with the smart sensor nodes to overcome the limitation of power supply.

## Acknowledgements

This study was supported by Smart Infra-Structure Technology Center granted by National Research Foundation of Korea, Harbor Remodeling Project funded by Korean Ministry of Land, Transport and Maritime Affairs, and Brain Korea 21 Program funded by Korean Ministry of Education, Science, and Technology. Also, the authors are indebted to Dr. G. Park of Los Alamos National Laboratory, USA and Prof. M.D. Todd of Univ. of California at San Diego, USA, for their technical supports.

## References

- Adams, R.D., Cawley, P., Pye, C.J. and Stone, B.J. (1978), "A vibration technique for non-destructively assessing the integrity of structures", *J. Mech. Eng. Sci.*, **20**(2), 93-100.
- Analog Devices Inc. (2009), *Datasheet of AD5933*, Available at <http://www.analog.com>.
- Bhalla, S. and Soh, C.K. (2003), "Structural impedance based damage diagnosis by piezo-transducers", *Earthq. Eng. Struct. D.*, **32**(12), 1897-1916.
- Cho, S., Yun, C.B., Lynch, J.P., Zimmerman, A.T., Spencer, B.F. and Nagayama, T. (2008), "Smart wireless sensor technology for structural health monitoring of civil structures", *Int. J. Steel Struct.*, **8**(4), 267-276.
- Jeyasehar, C.A. and Sumangala, K. (2006), "Damage assessment of prestressed concrete beams using Artificial Neural Network (ANN) approach", *Comput. Struct.*, **84**, 1709-1718.
- Kim, J.T., Na, W.B., Hong, D.S. and Park, J.H. (2006), "Global and local health monitoring of plate-girder bridges under uncertain temperature conditions", *Int. J. Steel Struct.*, **6**, 369-376.
- Kim, J.T., Park, J.H., Hong, D.S., Cho, H.M., Na, W.B. and Yi, J.H. (2009), "Vibration and impedance monitoring for prestress-loss prediction in PSC girder bridges", *Smart Struct. Syst.*, **5**(1), 81-94.
- Kim, J.T., Park, J.H., Hong, D.S. and Park, W.S. (2010), "Hybrid health monitoring of prestressed concrete girder bridges by sequential vibration-impedance approaches", *Eng. Struct.*, **32**, 115-128.
- Kim, J.T., Ryu, Y.S., Cho, H.M. and Stubbs, N. (2003a), "Damage identification in bean-type structures: frequency-based method vs mode-shape-based method", *Eng. Struct.*, **25**, 57-67.
- Kim, J.T., Yun, C.B., Ryu, Y.S. and Cho, H.M. (2004), "Identification of prestress-loss in PSC beams using modal information", *Struct. Eng. Mech.*, **17**(3-4), 467-482.
- Kim, J.T. (2001), "Crack detection scheme for steel plate-girder bridges via vibration-based system identification", *KSCE J. Civil Eng.*, **5**(1), 1-10.
- Kim, J.T., Lee, Y.K., Kim, J.H. and Baek, J.H. (2002), "GUI software system for damage identification in plate-girder bridges", *KSCE J. Civil Eng.*, **6**(2), 107-118.
- Kim, J.T., Yun, C.B. and Yi, J.H. (2003b), "Temperature effects on frequency-based damage detection in plate-girder bridges", *KSCE J. Civil Eng.*, **7**(6), 725-733.
- Krishnamurthy, V., Fowler, K. and Sazonov, E. (2008), "The effect of time synchronization of wireless sensors

- on the modal analysis of structures”, *Smart Mater. Struct.*, **17**, 1-13.
- Liang, C., Sun, F.P. and Rogers, C.A. (1994), “Coupled electromechanical analysis of adaptive material systems-determination of the actuator power consumption and system energy transfer”, *J. Intel. Mat. Syst. Str.*, **5**(1), 12-20.
- Lu, K.C., Loh, C.H., Yang, Y.S., Lynch, J.P. and Law, K.H. (2008), “Real-time structural damage detection using wireless sensing and monitoring system”, *Smart Struct. Syst.*, **4**(6), 759-777.
- Lynch, J.P., Sundararajan, A., Law, K.H., Kiremidjian, A.S., Kenny, T. and Carryer, E. (2003), “Embedment of structural monitoring algorithms in a wireless sensing unit”, *Struct. Eng. Mech.*, **15**(3), 385-297.
- Lynch J.P., Wang, W., Loh, K.J., Yi, J.H. and Yun, C.B. (2006), “Performance monitoring of the Geumdang Bridge using a dense network of high-resolution wireless sensors”, *Smart Mater. Struct.*, **15**, 1561-1575.
- Miyamoto, A., Tei, K., Nakamura, H. and Bull, J.W. (2000), “Behavior of prestressed beam strengthened with external tendons”, *J. Struct. Eng.*, **126**, 1033-1044.
- Mascarenas, D.L., Todd, M.D., Park, G. and Farrar, C.R. (2007), “Development of an impedance-based wireless sensor node for structural health monitoring”, *Smart Mater. Struct.*, **16**, 2137-2145.
- Nagayama, T. (2007), *Structural health monitoring using smart sensors*, Ph.D Dissertation, University of Illinois at Urbana-Champaign, UC, USA.
- Nagayama, T., Sim, S.H., Miyamori, Y. and Spencer, B.F. (2007), “Issues in structural health monitoring employing smart sensors”, *Smart Struct. Syst.*, **3**(3), 299-320.
- Park, G., Cudney, H. and Inman, D.J. (2000), “Impedance-based health monitoring of civil structural components”, *J. Infrastruct. Syst.-ASCE*, **6**(4), 153-160.
- Park, S., Ahmad, S., Yun, C.B. and Roh, Y. (2006), “Multiple crack detection of concrete structures using impedance-based structural health monitoring techniques”, *Exp. Mech.*, **46**(5), 609-618.
- Rice, J.A. and Spencer, B.F. (2008), “Structural health monitoring sensor development for the Imote2 platform”, *Proc. of SPIE*, **6932**.
- Ruiz-Sandoval, M., Nagayama, T. and Spencer, B.F. (2006) “Sensor development using Berkeley mote platform”, *J. Earthq. Eng.*, **10**(2), 289-309.
- Saiidi, M., Douglas, B. and Feng, S. (1994), “Prestress force effect on vibration frequency of concrete bridges,” *J. Struct. Eng.*, **120**, 2233-2241.
- Sohn, H., Farrar, C.R., Hemez, F.M., Shunk, D.D., Stinemates, D.W. and Nadler, B.R. (2003), *A Review of Structural Health Monitoring Literature: 1996-2001*, Los Alamos National Laboratory Report, LA-13976-MS, Los Alamos, NM
- Spencer, B.F., Ruiz-Sandoval, M.E. and Kurata, N. (2004), “Smart Sensing Technology: Opportunities and Challenges”, *Struct. Control Health Monit.*, **11**, 349-368
- Straser, E.G. and Kiremidjian, A.S. (1998) *A Modular, Wireless Damage Monitoring System for Structure*, Technical Report 128, John A. Blume Earthquake Engineering Center, Stanford University, Stanford, CA.
- Stubbs, N. and Osegueda, R. (1990), “Global non-destructive damage evaluation in solids”, *Int. J. Anal. Exp. Modal Anal.*, **5**(2), 67-79.
- Sun, F.P., Chaudhry, Z., Rogers, C.A. and Majmundar, M. (1995), “Automated real-time structure health monitoring via signature pattern recognition”, *Proceedings of the SPIE North American Conference on Smart Structures and Materials*, San Diego, CA.
- Yi, J.H. and Yun, C.B. (2004), “Comparative study on modal identification methods using output-only information”, *Struct. Eng. Mech.*, **17**(3-4), 445-446.
- Yun, C.B. and Bahng, E.Y. (2000) “Substructural identification using neural networks”, *Comput. Struct.*, **77**(1), 41-52.
- Wang, Y., Swartz, R.A., Lynch, J.P. and Law K.H. (2007), “Decentralized civil structural control using real-time wireless sensing and embedded computing”, *Smart Struct. Syst.*, **3**(3), 321-340.
- Zimmerman, A.T., Shiraishi, M., Swartz, R.A. and Lynch, J.P. (2008), “Automated modal parameter estimation by parallel processing within wireless monitoring systems”, *J. Infrastruct. Syst.- ASCE*, **14**(1), 102-113.